

Measurement of Mode I and Mode II Fracture Properties of Wood-Bonded Joints

J. Xavier^{a,*}, J. Morais^a, N. Dourado^a and M. F. S. F. de Moura^b

^a CITAB, University of Trás-os-Montes and Alto Douro, Engenharias I, Apartado 1013, 5001-801 Vila Real, Portugal

^b DEMec, FEUP, University of Porto, Rua Dr. Roberto Frias, 4200-465 Porto, Portugal

Received in final form 11 January 2011; revised 15 April 2011; accepted 15 April 2011

Abstract

In this work, the fracture characterisation of wood-bonded joints under pure mode I and mode II loading was performed. The tested material was maritime pine (*Pinus pinaster* Ait.) bonded with an epoxy adhesive. Two fracture mechanical tests were chosen: the double cantilever beam (DCB) for opening mode I loading, and the end-notched flexure (ENF) for sliding mode II loading. The compliance-based beam method (CBBM) was used for both mode I and mode II fracture, since the Resistance-curves can be obtained directly from the global mechanical response of the specimens (load–displacement curve), without crack monitoring during propagation. This data reduction scheme was validated by direct comparison with the modified experimental compliance method (MECM).

© Koninklijke Brill NV, Leiden, 2011

Keywords

Fracture mechanics, wood-bonded joints, compliance-based beam method, modified experimental compliance method, double cantilever beam (DCB) test, end-notched flexure (ENF) test

1. Introduction

Wood is a biological composite material formed by trees. At the macroscopic scale (0.1–1 m), wood is usually modelled as a homogenous and orthotropic material, with three axes of symmetry: the longitudinal direction (L) along the stem, and the radial (R) and tangential (T) directions on the transversal plane [1].

Wood and wood products represent important engineering materials. The use of adhesive technologies in wooden construction offers several advantages over solid-sawn wood, allowing a more efficient exploitation of forest resources. Moreover, it permits engineers to design lighter and more innovative structures that offer better

* To whom correspondence should be addressed. Tel.: +351 259 350 356; Fax: +351 259 350 356; e-mail: jmcx@utad.pt

performance. Although there have been great achievements in science and engineering of wood adhesion, characterization and modelling of bond strength of adhesives at adherend wood–wood interface remains an open issue. Veigel *et al.* [2] determined the specific fracture energy of spruce wood-bonded joints using the double cantilever beam (DCB) test. The fracture energy was directly obtained from the load–displacement curve of the DCB fracture test. The specific fracture energy was calculated by dividing the area under the load–displacement curve by the fracture surface area. In addition, fracture energy was determined using the direct compliance method. The authors concluded that fracture testing is appropriate for the characterization of adhesive performance. Davalos *et al.* [3] used the constant-taper contoured double cantilever beam (CDCB) test for mode-I fracture characterisation of wood–wood bonded interfaces to determine the critical loads for crack initiation and crack arrest, from which the respective critical strain energy release rates are obtained. This specimen allows a linear variation of compliance as a function of crack length, which simplifies the calculation of strain energy release rate. It has been concluded that this specimen is well suited for interface bond studies. Wang and Qiao [4] and Qiao *et al.* [5] used the tapered end-notched flexure (TENF) specimen for fracture characterization of wood–wood bonded joints under pure mode II loading. They demonstrated that an approximately constant rate of compliance *versus* crack length can be attained when a proper design is carried out. The authors concluded that the critical strain energy release rate in mode II of wood–wood bonded interfaces is properly determined by the proposed method. Singh *et al.* [6] used the dual actuator load (DAL) test for mixed mode fracture characterisation of wood-bonded joints. This test can be viewed as a combination of the DCB and end loaded split (ELS) test. The dual actuator instrument offers the possibility to apply both symmetrical and asymmetrical loading to the test specimen. It thus enables testing over a wide range of mode types from pure mode I to pure mode II. A global review of the works concerning fracture characterization of wood and wood bonded joints was presented by Conrad *et al.* [7].

The purpose of this paper is to present an experimental work about the identification of Resistance-curves (*R*-curves) under pure mode I and mode II of adhesively bonded wood joints. The determination of *R*-curves acquires special relevancy when the fracture process zone (FPZ) is not negligible. Effectively, in these cases the definition of crack initiation is dubious which can lead to an erroneous evaluation [8]. The *R*-curve is advantageous since it allows overcoming all of the difficulties related to identification of crack initiation because this curve includes all the information concerning the fracture process as is the case of FPZ development, crack starting advance and self-similar crack growth. The present work is focused on maritime pine (*Pinus pinaster* Ait.) bonded with an epoxy adhesive. Two fracture mechanical tests were used: the double cantilever beam (DCB) test to apply mode I loading, and the end-notched flexure (ENF) test for mode II loading. Recently, it has been demonstrated that both mode I and mode II *R*-curves can be obtained according to beam theory, without crack monitoring during propaga-

tion [9–11]. The so-called compliance-based beam method (CBBM) only requires the global load–displacement response of the specimen. Finally, this data reduction scheme was validated by direct comparison with the modified experimental compliance method (MECM).

2. Double Cantilever Beam Test

The double cantilever beam (DCB) test was used to evaluate fracture mechanical properties under mode I loading. A schematic representation of the DCB test is shown in Fig. 1. The specimen has a cross-section of $2h \times B$, the load was applied at a distance L from the specimen end, and there is a mid-height pre-cracked surface of initial length a_0 . Mode I fracture along the extension ($L-a_0$) was assumed to occur by applying a load P (originally perpendicular to the pre-cracked surface). In the course of the loading process the applied load (P), the displacement of its application point (δ) and the continuous crack length (a) were measured. The strain energy release rate in pure mode I (G_I) was then be determined from the Irwin–Kies formulation

$$G_I = \frac{P^2}{2B} \frac{dC}{da}, \quad (1)$$

where C is the compliance determined from the load–displacement curve

$$C = \frac{\delta}{P}. \quad (2)$$

Several methods have been proposed to determine the Resistance-curve (R -curve) from the DCB test (equation (1)). Two different data reduction schemes were applied in this work: (i) the compliance-based beam method (CBBM) [9]; (ii) the modified experimental compliance method (MECM) [10]. These methodologies are summarised in the following sections.

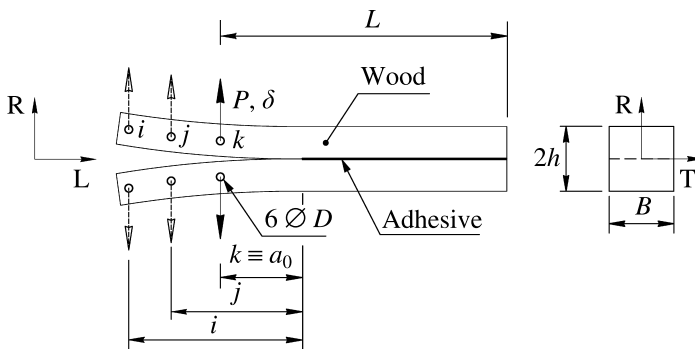


Figure 1. Double cantilever beam (DCB) test ($2h = 20$, $B = 20$, $L = 400$, $D = 3$, $i = 200$, $j = 150$, $k \equiv a_0 = 100$; unit: mm).

2.1. Compliance-Based Beam Method

The compliance-based beam method (CBBM) relies on the concept of an equivalent crack length, thus only requiring the measurement of the load–displacement (P – δ) curve during the fracture test. Therefore, this method represents a suitable alternative in applications where the definition and measurement of the crack length, a , during propagation is not accurate or possible. This is the case for wood and wood-bonded joints, where a non-negligible fracture process zone (FPZ) develops ahead of the crack tip. In wood, the toughening mechanisms consist mainly of micro-cracking, crack-branching and fibre-bridging [9]. In bonded joints, the ductility of the adhesive plays an important role in the definition of the FPZ size.

From the Timoshenko beam theory and Castigliano theorem the following equation can be obtained for the compliance of the DCB specimen

$$C = \frac{8a^3}{E_L B h^3} + \frac{12a}{5 B h G_{LR}}, \quad (3)$$

where E_L is the longitudinal modulus of elasticity and G_{LR} is the shear modulus in the LR plane. This equation does not take into account either the section rotation or the local stress concentration at the crack tip. Moreover, the coefficients of a in equation (3) are functions of the elastic properties of the specimen to be tested. To avoid additional experimental tests for the identification of these parameters, the concept of corrected flexural modulus (E_f) was proposed to replace the actual value of E_L . It was verified that the G_{LR} modulus has a negligible influence on G_I and a reference value can be used [9]. The E_f of each specimen can be obtained from equation (3) using the measured initial compliance (C_0) and the corrected initial crack length ($a_0 + \Delta$)

$$E_f = \left(C_0 - \frac{12(a_0 + \Delta)}{5 B h G_{LR}} \right)^{-1} \frac{8(a_0 + \Delta)^3}{B h^3}, \quad (4.1)$$

where Δ is the Williams correction term [12]

$$\Delta = h \sqrt{\frac{E_f}{11 G_{LR}} \left[3 - 2 \left(\frac{\Gamma}{1 + \Gamma} \right)^2 \right]}, \quad (4.2)$$

$$\Gamma = 1.18 \frac{\sqrt{E_f E_T}}{G_{LR}}, \quad (4.3)$$

where E_T is the tangential modulus of elasticity. An iterative procedure was used to solve equations (4) in order to obtain a converged value of E_f (this convergence is reached in only a few iterations). It is worth noting that this procedure takes into account eventual inaccuracies of beam theory and is less sensitive to experimental errors (initial crack length measurements and variability of elastic properties).

During propagation an equivalent crack length ($a_{eq} = a + \Delta + \Delta a_{FPZ}$) is considered to account for the FPZ effect at the crack tip. The value of a_{eq} during

propagation was obtained from equation (3) using the Matlab[®] software considering a_{eq} and E_f instead of a and E_L , respectively. Following this procedure, the a_{eq} is a function of current compliance which is influenced by root rotation effects and fracture process zone. Consequently, these effects are indirectly taken into account by means of a_{eq} .

Combining equations (1) and (3), the following expression for the strain energy release rate in mode I is obtained

$$G_I = \frac{6P^2}{B^2h} \left(\frac{2a_{eq}^2}{E_f h^2} + \frac{1}{5G_{LR}} \right). \quad (5)$$

2.2. Modified Experimental Compliance Method

In the experimental compliance method (ECM) the compliance is given as a function of the crack length by the following empirical expression

$$C = \alpha a^\beta, \quad (6)$$

where α and β are parameters determined experimentally. By substituting equation (6) into equation (1) and considering the definition of equation (2), the strain energy release rate G_I is given by

$$G_I = \frac{\beta P \delta}{2Ba} \quad (7)$$

Considering the uncertainty that can exist for some materials on measuring the crack length during propagation, the ECM can be modified for determining the R -curve from only the P – δ curve. This method is called the modified experimental compliance method (MECM). The parameters in equation (6) were determined by fitting a straight line to the $\log_{10} C$ – $\log_{10} a$ experimental data points using least-squares regression

$$\log_{10} C = \log_{10} \alpha + \beta \log_{10} a, \quad (8)$$

where C represents the compliance obtained for a given initial crack length a in a logarithm to base 10. Experimentally, this set of data (equation (8)) requires carrying out preliminary tests on the DCB specimen (without crack propagation), in which the elastic P – δ curve (compliance value) is measured for several initial crack lengths, as illustrated in Fig. 1 (loading lines i , j and k). The fracture mechanical test was then carried out on the same specimen for crack propagation (loading line k). At each point of the resulting P – δ curve (actual compliance value) an equivalent crack length (a_{eq}) was then estimated from equation (8). The R -curve was then determined from equation (7) by replacing the crack length (a) with the estimated equivalent crack length (a_{eq}).

3. End-Notched Flexure Test

The end-notched flexure (ENF) test was used to determine the strain energy release rate in pure mode II. A schematic representation of the ENF test is shown in Fig. 2.

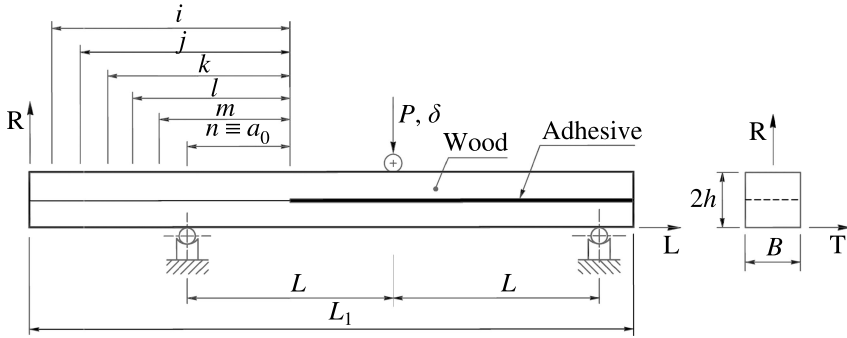


Figure 2. End-notched flexural (ENF) test ($2h = 20$, $B = 20$, $L = 230$, $L_1 = 610$, $i = 212$, $j = 202$, $k = 192$, $l = 182$, $m = 172$, $n \equiv a_0 = 162$; unit: mm).

A pre-cracked beam specimen was submitted to a three-point bending test in which predominant shear loading was induced at the crack tip. The initial crack length (a_0) was typically greater than $0.7 L$ in order to ensure stable crack propagation [13] and L was the mid-span distance (Fig. 2).

The data reduction schemes based on the compliance-based beam method (CBBM) and modified experimental compliance method (MECM) were applied to the ENF test as described in the following sections.

3.1. Compliance-Based Beam Method

Assuming the beam theory with shear effects, the specimen compliance during crack propagation can be written as

$$C = \frac{3a_{eq}^3 + 2L^3}{12E_f I} + \frac{3L}{5G_{LR}A}, \quad (9)$$

where $a_{eq} = a + \Delta a_{FPZ}$ (Δa_{FPZ} is the crack length correction accounting for the FPZ effect), $A = 2hB$ and I is the second moment of area. It should be noted that root rotations effects are less important in the ENF relatively to DCB test which means that a specific correction Δ was not considered in this case. As a result, the effect of root rotation is also included in the corrected modulus, which simplifies the method when applied to ENF test. Considering the initial crack length (a_0) and compliance (C_0), the flexural modulus of the specimen can be obtained from equation (9)

$$E_f = \frac{3a_0^3 + 2L^3}{12I} \left(C_0 - \frac{3L}{5G_{LR}A} \right)^{-1}. \quad (10)$$

During propagation the equivalent crack length can be obtained from equations (9) and (10)

$$a_{eq} = a + \Delta a_{FPZ} = \left[\frac{C_{corr}}{C_{0corr}} a_0^3 + \frac{2}{3} \left(\frac{C_{corr}}{C_{0corr}} - 1 \right) L^3 \right]^{1/3} \quad (11.1)$$

with

$$C_{\text{corr}} = C - \frac{3L}{5G_{\text{LR}}A} \quad \text{and} \quad C_{0_{\text{corr}}} = C_0 - \frac{3L}{5G_{\text{LR}}A}. \quad (11.2)$$

The critical strain energy release rate G_{IIc} can then be obtained considering the equation of Irwin–Kies (equation (1))

$$G_{\text{IIc}} = \frac{9P^2}{16B^2E_f h^3} \left[\frac{C_{\text{corr}}}{C_{0_{\text{corr}}}} a_0^3 + \frac{2}{3} \left(\frac{C_{\text{corr}}}{C_{0_{\text{corr}}}} - 1 \right) L^3 \right]^{2/3}. \quad (12)$$

This data reduction method does not require crack length measurement during propagation, since it was based on an equivalent crack concept (equation (11)). Furthermore, a flexural modulus (E_f) was determined from the initial compliance (C_0) measured experimentally, avoiding an additional independent test method. A reference value of G_{LR} can be systematically used since the value of G_{IIc} was not significantly affected [11]. Moreover, the CBBM accounts for the non-negligible energy dissipation which takes place in the FPZ, as this material-weakening process influences specimen compliance.

3.2. Modified Experimental Compliance Method

The experimental compliance method (ECM) is based on the assumption that the compliance of ENF specimen is given as a function of the crack length by the following expression [14]

$$C = \eta + \lambda a^3, \quad (13)$$

where η is the uncracked compliance and λ is the slope of a plot of compliance *versus* the cube of crack length. Equation (13) may be differentiated and substituted into the equation of Irwin–Kies (equation (1)) to give the strain energy release rate G_{II}

$$G_{\text{II}} = \frac{3\lambda P^2 a^2}{2B}. \quad (14)$$

Considering the difficulty in measuring the crack length during propagation, the modified experimental compliance method (MECM) can be used for determining the R -curve from only the P – δ curve, in a similar way as was presented above for DCB tests. Accordingly, preliminary tests on each ENF specimen was carried out without crack propagation, in which the compliance C was measured for several initial crack lengths (Fig. 2). The constants in equation (13) were determined by fitting a straight line to the C – a^3 experimental data points using a least-squares regression. Afterwards, the fracture test was performed on the same specimen. At each point of the resulting P – δ curve (actual compliance value) an equivalent crack length (a_{eq}) was then estimated from equation (13). Finally, the R -curve was determined from equation (14) by replacing the crack length (a) with the equivalent crack length (a_{eq}).

4. Experimental Work

4.1. Material and Specimens

The material used in this work was maritime pine (*Pinus pinaster* Ait.) taken from a single tree (origin: Portugal). Beams for both DCB (Fig. 1) and ENF (Fig. 2) specimens were cut from mature wood (outermost region of the stem). Specimens of wood-bonded joints were then prepared using an epoxy adhesive (Araldite® 2015), for both mode I (12 specimens) and mode II (10 specimens) test configurations. Reference values of modulus of elasticity (E_L) and shear modulus (G_{LR}) of *P. pinaster* are 1.91 GPa and 1.04 GPa, respectively [15].

The dimensions of the DCB specimen were $2h = 20$ mm, $B = 20$ mm, $L = 400$ mm and $a_0 = 100$ mm (Fig. 1). According to MECM (Section 2.2) the calibration $C = f(a)$ was executed performing compliance measurements for three successive initial crack lengths ($i > j > k$ in Fig. 1), with relative distance among them of 50 mm. It is worth noting that holes i , j and k (Fig. 1) are machined in this order, just when the tests were to be performed at each location. For the pre-cracks i and j , a slight load must be applied (linear elastic domain), since the aim is only the measurement of the respective initial compliance C without introducing any damage. At the end, the fracture test was carried out considering the pre-crack $k \equiv a_0$. The applied load was transferred to the DCB specimen by means of two steel pins with a diameter $D = 3$ mm, inserted into the drilled holes at the specimen end arms (Fig. 1).

The dimensions of the ENF specimen were $2h = 20$ mm, $B = 20$ mm, $L = 230$ mm, $L_1 = 610$ mm and $a_0 = 162$ mm (Fig. 2). The ratio of pre-crack length to mid-span (a_0/L) was about 0.7 to attain the conditions of self-similar crack growth [11]. Two sheets of Teflon® with a pellicle of lubricant between them were placed in the mid-thickness pre-cracked surface in order to reduce the friction effect during crack propagation in mode II. The preliminary tests of compliance calibration were performed in each ENF specimen for five successive initial crack lengths ($i > j > k > l > m$ in Fig. 2), just by sliding the specimen over the supports, without introducing any damage. At the end, the fracture test was carried out considering the pre-crack $n \equiv a_0$.

Specimens were kept in the laboratory in order to reach their equilibrium state before testing. The mean value of oven-dry specific density of the specimens (determined as the ratio between the oven-dry weight and green volume) was found to be 0.60 g/cm^3 , with a coefficient of variation of 10.8%. Using the oven-dry method, a moisture content of 11% was estimated for the specimens during the tests.

4.2. Fracture Mechanical Tests

The DCB and the ENF fracture mechanical tests were carried out in a conventional screw-driven Instron® 1125 testing machine at crosshead displacement rate of 5 mm/min. The applied load was measured by means of a 100 kN load cell. The load (P) and the crosshead displacement of the testing machine (δ) were recorded

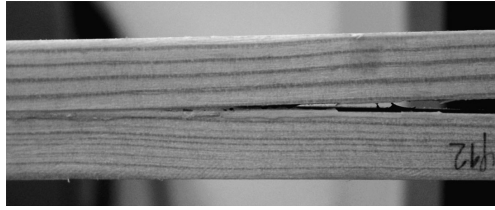


Figure 3. Crack propagation on a DCB specimen loaded in mode I.

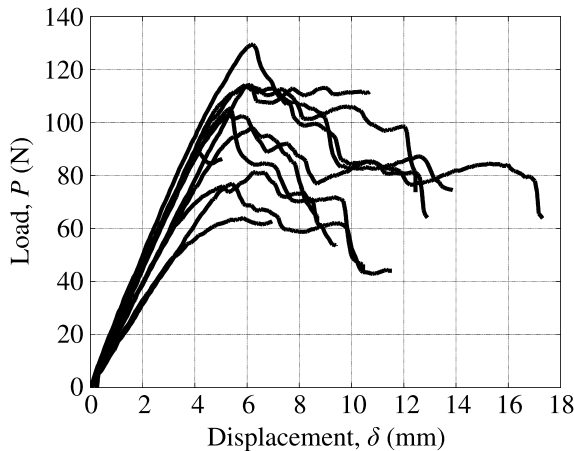


Figure 4. Load–displacement curves of DCB specimens.

with a frequency of 5 Hz using a Spider[®] 8 HBM acquisition system. The crack length during testing was not measured due to difficulties in defining the crack tip location during propagation, as shown in Fig. 3 for the case of a DCB specimen. This observation supports the utilisation of the CBBM and the MECM data reduction schemes for the evaluation of the *R*-curve both on the DCB and on the ENF fracture mechanical tests.

5. Results and Discussion

5.1. Double Cantilever Beam Test

The raw data measured in the DCB test was the applied load and cross-head displacement (Fig. 4). The variation observed in Fig. 4 is typical for a biological material like wood. Taking into account the MECM, for each DCB specimen the load–displacement curve was measured by successively shifting the point of application of the applied load at three distinct positions (*i*, *j* and *k* in Fig. 1). Such results are shown in Fig. 5(a), where the first two curves (*i* and *j* in Figs 1 and 5(a)) correspond to preliminary tests without crack propagation, and the last curve (*k* in Figs 1 and 5(a)) resulting from the complete mode I fracture mechanical test. The linear part of the three curves (i.e., the maximum number of *P*– δ points for which

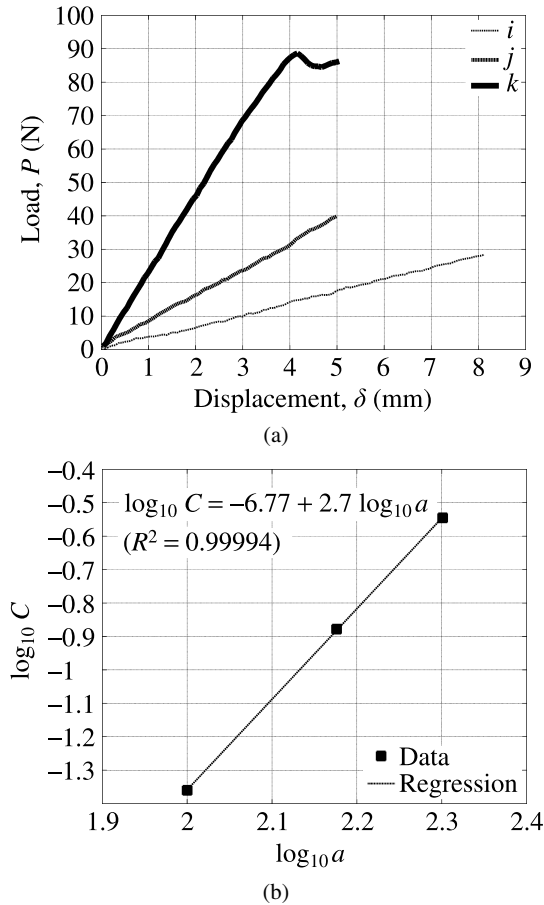


Figure 5. MECM scheme for DCB specimen: (a) load–displacement (P – δ) curves; (b) Compliance–crack length ($\log_{10} C$ – $\log_{10} a$) data points and compliance calibration line.

the linear regression gives a coefficient of determination $R^2 \geq 0.999$) was used for the construction of the compliance calibration curve (equation (8)) presented in Fig. 5(b). In this example $\log_{10} \alpha = -6.77$ and $\beta = 2.7$, where β represents the slope of the straight linear of the least-squares regression.

Both CBBM (equation (5)) and MECM (equation (7)) were applied to the DCB specimen in order to estimate the R -curve. A comparison between both methods is shown in Fig. 6 for a typical DCB specimen. Good agreement was observed between both methods in spite of a slightly lower plateau for the CBBM with regard to the MECM. This can be explained by the FPZ. Effectively, in the CBBM the FPZ is indirectly accounted for, which does not happen in the MECM since the calibration curve is obtained in the elastic domain. The critical strain energy release rate was then evaluated from the R -curves. The results are summarised in Table 1, for both CBBM and MECM data reduction schemes. Two definitions were chosen for evaluating the strain energy release rate: (i) $G_{I, P_{\max}}$ was considered at the max-

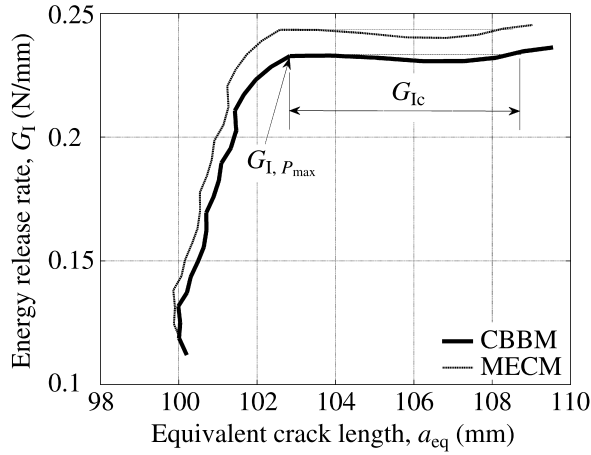


Figure 6. Comparison between CBBM and MECM schemes for determining the Resistance-curve of DCB specimen.

Table 1.

Fracture energy obtained from DCB specimens by means of CBBM and MECM

Specimen	P_{\max} (N)	$G_{I, P_{\max}}$ (N/mm)		G_{Ic} (N/mm)			
		CBBM	MECM	CBBM		MECM	
				Mean	CV (%)	Mean	CV (%)
1	105.3	0.351	0.361	0.301	5.7	0.306	6.1
2	64.0	0.219	0.214	0.219	0.4	0.214	0.3
3	97.8	0.370	0.402	0.370	0.5	0.402	0.5
4	114.1	0.416	0.408	0.421	1.2	0.412	1.1
5	102.9	0.271	0.265	0.256	3.2	0.248	3.6
6	102.8	0.233	0.243	0.233	0.8	0.242	0.8
7	115.1	0.298	0.274	0.299	0.4	0.274	0.3
8	105.2	0.497	0.515	0.465	4.1	0.478	4.5
9	102.0	0.450	0.460	0.440	2.3	0.448	2.5
10	105.2	0.337	0.344	0.339	0.5	0.346	0.4
11	106.5	0.416	0.420	0.417	0.2	0.421	0.2
12	104.6	0.331	0.337	0.321	1.8	0.326	2.1
Mean		0.349	0.354	0.340		0.343	
CV (%)		24.61	26.04	24.39		25.73	

imum load value; (ii) G_{Ic} was determined as the mean value over a plateau region of the R -curve, as illustrated in Fig. 6. The convergence to a critical strain energy release rate was assessed by the coefficient of variation determined over the value in the plateau of the R -curves. In conclusion, good agreement was observed between CBBM and MECM data reduction schemes (Table 1). Therefore, the crack equivalent concept used in developing the CBBM was validated from this direct

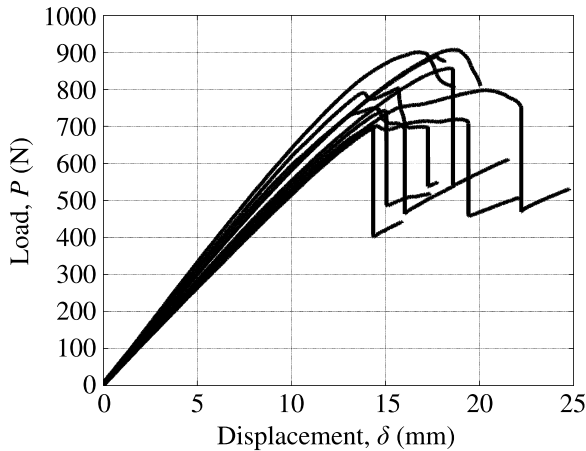


Figure 7. Load–displacement curves of ENF specimens.

comparison between different experimental approaches. Moreover, the mean value of $G_{I,P_{\max}}$ can be taken as a practical measure of the mode I critical strain energy release rate.

5.2. End-Notched Flexure Test

The load–displacement curves measured experimentally on the ENF specimens are shown in Fig. 7. Some scatter is also observed — this is typical for this material. On the other hand, Fig. 8 illustrates the application of MECM for ENF test. The load–displacement curve (Fig. 8(a)) was registered for five initial crack lengths (Fig. 2) by successively displacing the specimen over the supports, before carrying out the fracture test for $n \equiv a_0$. This experimental data was then used to obtain the compliance calibration curve (equation (13)) showed in Fig. 8(b).

The CBBM (equation (12)) and MECM (equation (14)) were applied in order to calculate the fracture energy in mode II. The typical R -curves obtained according to these identification schemes are presented in Fig. 9. The fracture energy was measured both at the maximum load ($G_{II,P_{\max}}$) and over the plateau of the R -curve (G_{IIc}) corresponding to self-similar stable crack propagation. These results are presented in Table 2 for all tested ENF specimens. The existence of a plateau in R -curve can be confirmed from the low scatter over G_{IIc} as measured by the coefficient of variation. Moreover, a good agreement was observed between CBBM and MECM data reduction schemes. These findings confirm the validity of the CBBM for fracture characterisation in mode II from the ENF specimen.

6. Conclusions

In this work the characterisation of fracture energy under pure mode I and mode II of wood-bonded joints was investigated. The double cantilever beam (DCB) test was chosen for pure mode I loading, whilst the end-notched flexure (ENF) was used

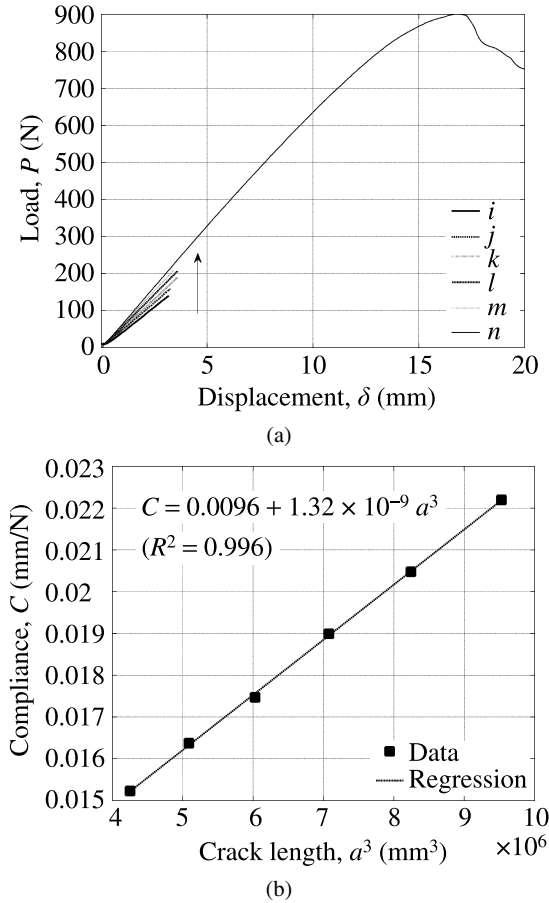


Figure 8. MECM scheme for ENF specimen: (a) load–displacement (P – δ) curves; (b) Compliance–crack length (C – a^3) data points and compliance calibration line.

for pure mode II loading. Beam specimens were manufactured from maritime pine (*Pinus pinaster* Ait.), and bonded by means of an epoxy adhesive. A comparison between the compliance-based beam method (CBBM) and the modified experimental compliance method (MECM) for data reduction schemes was performed. The main feature of the CBBM is that the Resistance-curves can be determined directly from the global mechanical response of the specimens (load–displacement curve), without crack monitoring. For the wood-bonded joint specimens, this was advantageous since the crack length during propagation cannot be measured without ambiguity in both fracture mechanical tests. The CBBM was experimentally validated by direct comparison with the MECM. Good agreement was achieved between these identification methods.

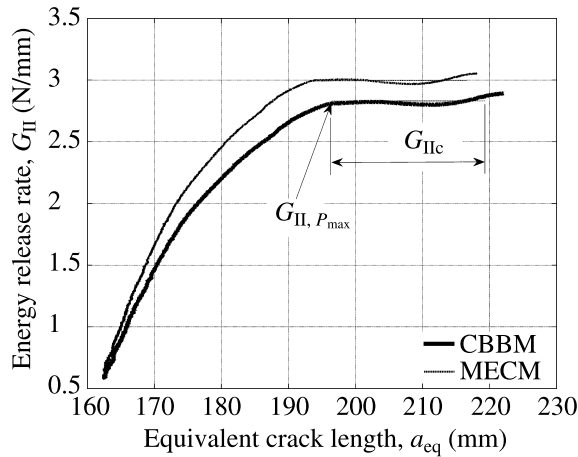


Figure 9. Comparison between CBBM and MECM schemes for determining the Resistance-curve of ENF specimen.

Table 2.
Fracture energy obtained from ENF specimens by means of CBBM and MECM

Specimen	P_{max} (N)	$G_{II, P_{max}}$ (N/mm)		G_{IIc} (N/mm)			
		CBBM	MECM	CBBM		MECM	
				Mean	CV (%)	Mean	CV (%)
1	901.4	2.731	2.921	2.858	1.9	3.024	1.5
2	907.9	3.047	3.065	3.117	0.8	3.132	0.8
3	890.5	2.781	2.730	2.816	0.8	2.764	0.8
4	857.4	2.785	2.804	2.815	0.4	2.835	0.4
5	721.3	1.879	1.987	1.878	0.1	1.987	0.1
6	803.6	2.268	2.119	2.217	2.4	2.089	2.5
7	701.9	1.703	1.631	1.698	0.2	1.626	0.2
8	720.0	2.526	2.289	2.576	1.1	2.339	1.2
9	799.0	3.045	3.006	3.175	2.0	3.138	2.1
10	749.8	1.881	1.653	1.980	3.2	1.762	3.9
Mean		2.464	2.420	2.513		2.470	
CV (%)		20.31	22.88	21.17		23.46	

Acknowledgement

The authors would like to thank the Portuguese Foundation for Science and Technology for supporting this work, through the research project PTDC/EME-PME/114443/2009 and the *Ciência2008* program.

References

1. I. Smith, E. Landis and M. Gong, *Fracture and fatigue in Wood*. John Wiley and Sons, Chichester (2003).
2. S. Veigel, J. Follrich, W. Gindl-Altmutter and U. Müller, *Eur. J. Wood Wood Prod.* In press. DOI: 10.1007/s00107-010-0499-6.
3. J. Davalos, P. Madabhushi-Raman and P. Qiao, *Eng. Fract. Mech.* **58**, 173–192 (1997).
4. J. Wang and P. Qiao, *J. Compos. Mater.* **37**, 875–897 (2003).
5. P. Qiao, J. Wang and J. F. Davalos, *Int. J. Solids Struct.* **40**, 1865–1884 (2003).
6. H. K. Singh, A. Chakraborty, C. E. Frazier and D. A. Dillard, *Holzforschung* **64**, 353–361 (2010).
7. M. P. C. Conrad, G. D. Smith and G. Fernlund, *Wood Fiber Sci.* **36**, 26–39 (2004).
8. N. Dourado, S. Morel, M. F. S. F. de Moura, G. Valentin and J. Morais, *Composites Part A* **39**, 415–427 (2008).
9. M. F. S. F. de Moura, J. J. L. Morais and N. Dourado, *Eng. Fract. Mech.* **75**, 3852–3865 (2008).
10. N. Dourado, M. F. S. F. de Moura, J. J. L. Morais and M. Silva, *Holzforschung* **64**, 119–126 (2010).
11. M. F. S. F. de Moura, M. A. L. Silva, A. B. de Morais and J. J. L. Morais, *Eng. Fract. Mech.* **73**, 978–993 (2006).
12. J. G. Williams, The fracture mechanics of delamination tests, *J. Strain Anal.* **24**, 207–214 (1989).
13. L. A. Carlsson, J. W. J. Gillespie and R. B. Pipes, *J. Compos. Mater.* **20**, 594–604 (1986).
14. P. Davies, Protocols for interlaminar fracture testing of composites. ESIS-Polymers & Composites Task Group, IFR-EMER, Centre de Brest (1993).
15. J. C. Xavier, N. M. Garrido, M. Oliveira, J. L. Morais, P. P. Camanho and F. Pierron, *Composites Part A* **35**, 827–840 (2004).